TÜBİTAK

Turkish Journal of Chemistry

http://journals.tubitak.gov.tr/chem/

Research Article

Turk J Chem
(2016) 40: 54 – 64

doi:10.3906/kim-1501-69

Density functional study of the structure and water adsorption activity of an $Al_{30}O_{30}$ star-shaped alumina nanocage

Mehdi ZAMANI*
School of Chemistry, Damghan University, Damghan, Iran

Received: 21.01.2015 • **Accepted/Published Online:** 07.06.2015 • **Final Version:** 05.01.2016

Abstract: Molecular and electronic structures of a novel $Al_{30}O_{30}$ star-shaped alumina nanocage (SANC) were studied using the recently developed CAM-B3LYP density functional method. Comparison of the stretching vibrational modes of this compound with the corresponding modes related to an $Al_{20}O_{30}$ perfect cage and $Al_{50}O_{75}$ tubular alumina nanomaterials showed a shift to lower frequencies, while the bending modes moved to higher frequencies. The highest occupied molecular orbital (HOMO) of the SANC had 65% nonbonding character, whereas the lowest unoccupied molecular orbital (LUMO) was 72% antibonding. The HOMO and LUMO of the SANC arose mostly from Al *3s* and *2p* atomic orbitals. The theoretically estimated energy gap for this compound was 4.4 eV, which is lower than those for the alumina nanocage (ANC) and nanotube (ANT). The SANC with internal and external diameters of 5.7 and 6.2 Å had potential to interact with water molecule from sites Al(I) in the openings of the cage, Al(II) in the internal pore, and Al(III) in the external arms. The relative water adsorption activity of these sites was Al(I) > Al(III) >>> Al(II). The SANC can be introduced as a novel alumina nanostructure with lower stability and higher activity than well-known alumina materials.

Key words: Alumina, nano, HOMO, LUMO, DFT

1. Introduction

Due to the broad applications of cage and tubular inorganic nanostructures, it is important to study these compounds. They can be used for energy storage, sensing devices, drug delivery, medicine, and catalysis.[1–5] Recently, numerous theoretical studies on this topic have been reviewed by Bromley et al.[6,7] Moreover, several research groups have reviewed the experimental findings about these novel nanomaterials.[1–5,8–14]

Alumina is an inorganic nanostructure with excellent catalytic performance. Due to the thermal, chemical, and mechanical stability of alumina, this compound is widely used in industry.[15] Many different shapes of alumina nanostructures such as nanoparticles,[16] nanocapsules,[17] nanowires,[18] nanotrees,[19] nanorods,[20,21] nanochannels,[22] and nanotubes[23–36] have been prepared and characterized in recent years. Theoretical studies play an important role in determination of the structural and electronic properties of these compounds.[37–49]

The small alumina nanoclusters were widely studied in the literature.[37–41] For instance, Rahane et al.[37] have studied the atomic structures, growth behavior, and vibrational and electronic properties of these nanomaterials. The best performance was obtained for 4- and 6-membered rings isomers with the lowest energy.[37] Sun et al.[40] have studied the structure and stability of alumina clusters and their practical application

*Correspondence: m.zamani@du.ac.ir

for hydrogen adsorption. They found a global energy minimum for small clusters as perfect cages. For larger clusters, the cage-dimer and then an onion-like structure is more favorable.[40] Gu and co-workers studied the stability and bonding properties of single-cage and core-shell cage alumina nanoclusters.[41] The core-shell clusters were found to be more stable than corresponding single-cage clusters that predominate in the medium-sized clusters.[41]

The structural and electronic properties as well as the catalytic activity of alumina surface have been studied at nanoscale,[45–47] and in nanochannels,[46] nanocages,[48] and nanotubes.[49] Each nanochannel is composed of two platelets like nanosized alumina surfaces joined together.[46] The size of the cavity in the lowest energy minimum alumina nanochannel is 4 Å,[46] which is sufficient for encapsulating the small molecules. The calculated electronic structure and simulated scanning tunneling microscopy images of an $Al_{20}O_{30}$ alumina nanocage (ANC) predicted that this compound with a pore size of 7.2 Å has a greater tendency to make endohedral complexes.[48] Therefore, ANC has potential applications such as space confined nanoreactors, drug delivery, nanocapsules, and gas storage.[48] The difficulty in putting a single molecule inside the perfect cage is the big problem with using an ANC as a molecular container. The purpose of the present work was to solve this problem through the molecular design of a novel $Al_{30}O_{30}$ star-shaped alumina nanocage (SANC) with an internal pore for the capturing as well as two openings for the entering and exiting of the small molecules. The structural and electronic properties of the SANC were analyzed and compared to the corresponding data for an alumina perfect nanocage and nanotube. The interaction of a water molecule with its all active sites was examined by DFT calculations to identify the active site of this compound.

2. Results and discussion

In this study, the molecular structure and electronic properties of an $Al_{30}O_{30}$ SANC were analyzed using CAM-B3LYP density functional combined with 6-31G** basis set for oxygen and LanL2DZ effective core potential basis set for aluminum. This level of theory was written as CAM-B3LYP/6-31G**/LanL2DZ on the basis of previous assignments.[48–50] More details on the computational procedure are given in the computation section. The optimized structure of the SANC with C_{6h} symmetry is shown in Figure 1. The internal and external diameters of this molecule were 5.7 and 6.2 Å, respectively, on the basis of the optimized geometry calculated via CAM-B3LYP/6-31G**/LanL2DZ level of theory. Different aluminum and oxygen active sites of SANC were labeled with the roman numbers I to III in Figure 1. The bond lengths between Al(I) and O(I) atoms in the openings of cage are 1.698 and 1.706 Å, which are shorter than Al(I)–O(II) (1.742 Å), Al(II)–O(II) (1.942 Å), and Al(II)–O(III) (1.965 Å) bonds in the internal pore as well as Al(III)–O(III) (1.935 Å) and Al(III)–O(II) (2.000 Å) bonds in the external arms of the SANC. The latter bonds are longer than the Al–O distance in an $Al_{20}O_{30}$ alumina nanocage (1.716 Å)[48] and $Al_{50}O_{75}$ nanotube, i.e. 1.706 and 1.713 Å,[49] respectively.

Figure 2 shows the infrared (IR) spectra of the $Al_{30}O_{30}$ SANC calculated at CAM-B3LYP/6-31G**/LanL2DZ level of theory in comparison to an $Al_{20}O_{30}$ ANC and $Al_{50}O_{75}$ ANT. The observed bands at 1037 and 851 cm^{-1} are assigned to the stretching vibrations of Al–O bonds related to the openings and internal pore of the SANC, respectively. The modes observed at 598, 426, and 240 cm^{-1} are due to the bending vibrations of Al–O bonds in the openings of the SANC. The bending vibrations of external arms are seen at 567, 522, 468, and 304 cm^{-1}. The base peak in the IR spectra of the perfect alumina nanocage (1087 cm^{-1}) and nanotube (1084 cm^{-1}) is related to the stretching vibrations of Al–O bonds of the whole molecule. The additional bands observed at 1036, 1104, and 1116 cm^{-1} for ANT are assigned to the stretching vibrations

of Al–O bonds corresponding to the end cap, hemisphere cap, and center of the nanotube, respectively. The bending vibrations of Al–O bonds for the ANC appear at 436, 400, and 280 cm^{-1}, while for the ANT they are at 469, 421, 396, 373, 346, and 297 cm^{-1}. The stretching vibrational modes of the SANC were compared with the corresponding modes related to perfect cage and tubular alumina nanomaterials, which show a shift to lower frequencies. Meanwhile, the bending modes move to higher frequencies.

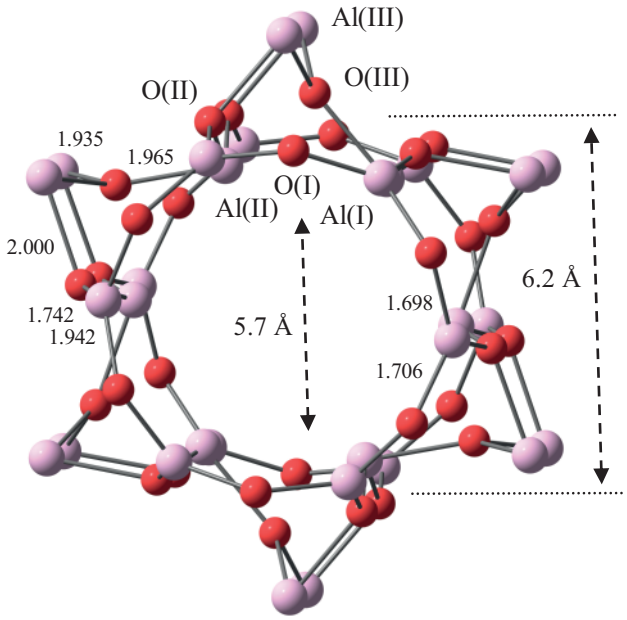

Figure 1. The optimized geometry of the star-shaped alumina nanocage calculated by CAM-B3LYP/6-31G**/LanL2DZ level of theory.

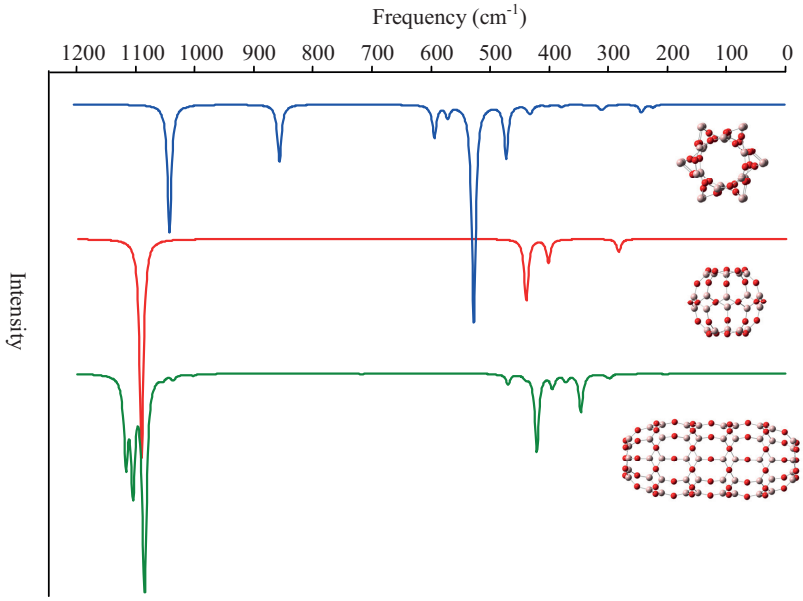

Figure 2. IR spectra for various alumina nanostructures, i.e. perfect nanocage (middle), nanotube (bottom), and star-shaped nanocage (top) calculated by CAM-B3LYP/6-31G**/LanL2DZ level of theory.

The total density of state (DOS) of the $Al_{30}O_{30}$ SANC calculated at CAM-B3LYP/6-31G**/LanL2DZ level of theory in comparison to $Al_{20}O_{30}$ ANC and $Al_{50}O_{75}$ ANT is shown in Figure 3. The valence band corresponding to the occupied orbitals of the ANC and ANT is seen at about –9 to –18 eV. This region mainly consists of O *2p* atomic orbitals. The conduction band related to the virtual orbitals of ANC and ANT is seen above –1 eV and is mainly composed of Al *3s* atomic orbitals. The valence band of the SANC appears in the region from –6 to –17 eV. The new band below the original valence band edge between –6 and –9 eV corresponds to Al *3s* and *2p* atomic orbitals. The main molecular orbitals of the SANC in this region are shown in Figure 4. The conduction band of the SANC with the contribution of Al *3s* and *2p* atomic orbitals appears above –1.7 eV. More important molecular orbitals of SANC in this region are indicated in Figure 5.

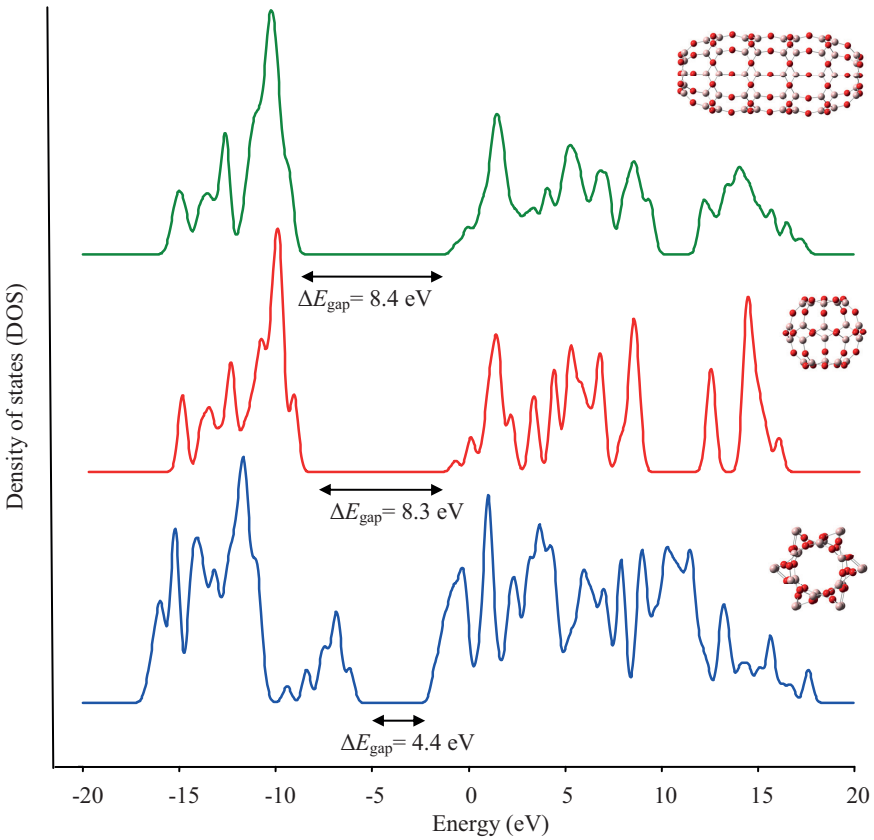

Figure 3. DOS diagrams for various alumina nanostructures, i.e. perfect nanocage (middle), nanotube (top), and star-shaped alumina nanocage (bottom) calculated by CAM-B3LYP/6-31G**/LanL2DZ level of theory. The positions of Fermi level are –9.3, –9.1, and –6.1 eV, respectively.

The highest occupied molecular orbital (HOMO) of the SANC is twofold degenerate with E_{1u} symmetry (Figure 4) and the lowest occupied molecular orbital (LUMO) is nondegenerate with A_u symmetry (Figure 5). The orbital energies of the HOMO and LUMO in CAM-B3LYP/6-31G**/LanL2DZ level of theory are –6.14 and –1.72 eV, respectively. As shown in Figures 4 and 5, the electron density is delocalized inside the cage with the first one over the Al(II) sites in the internal pore and the second one over the Al(I) sites in the openings of the cage. The calculated natural atomic orbitals analysis can predict that the HOMO and LUMO of the SANC arise mostly from Al *3s* and *2p* atomic orbitals. The canonical molecular orbital analysis predicts that the HOMO of the SANC has 65% nonbonding character, while the LUMO is 72% antibonding.

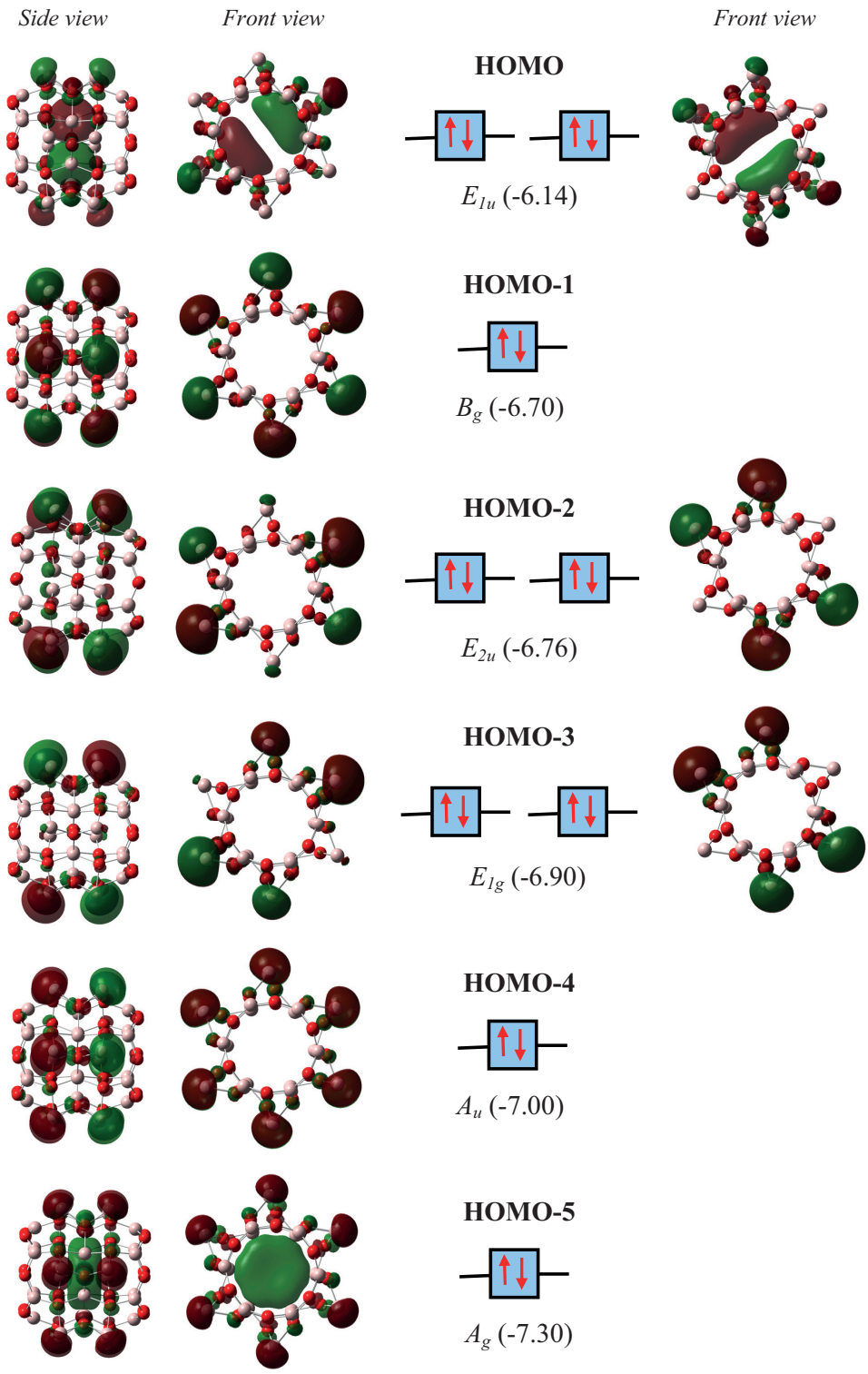

Figure 4. Molecular orbital shape and energy (eV) for the six highest occupied molecular orbitals of the star-shaped alumina nanocage calculated by CAM-B3LYP/6-31G**/LanL2DZ level of theory.

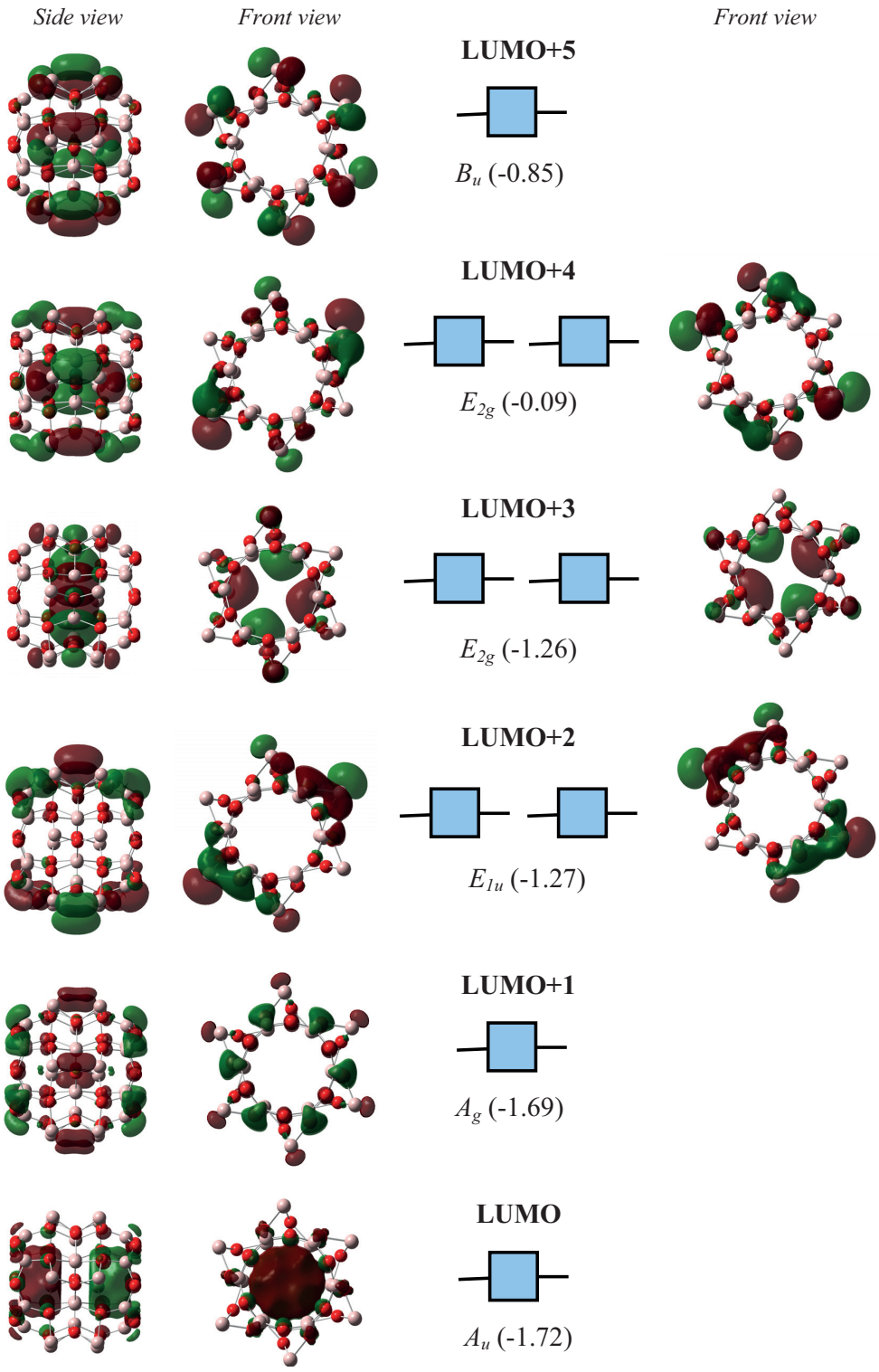

Figure 5. Molecular orbital shape and energy (eV) for the six lowest unoccupied molecular orbitals of the star-shaped alumina nanocage calculated by CAM-B3LYP/6-31G**/LanL2DZ level of theory.

The theoretically estimated energy separation between the HOMO and LUMO, which can be called the energy gap (ΔE_{gap}), for the SANC is 4.4 eV. This value is lower than those calculated for the alumina nanocage and nanotube (> 8 eV) (Figure 3). Since there is no experimental evidence about the electronic structure of the SANC in the literature, this value is comparable to the experimentally measured ΔE_{gap} for the bulk structure of γ-alumina (7.0 eV)[51] and α-alumina (8.8 eV).[52]

The relative stability of various types of alumina nanostructures with molecular formula Al_nO_m can be estimated by the calculation of binding energy per atom (BE/atom) in the cluster (refer to Eq. (1) in the computation section). This procedure is widely used in the literature for predicting the relative stability of various nanostructures with different molecular formulae.[37,40,53,54] The calculated BE/atom for $Al_{30}O_{30}$ SANC is 4.54 eV, which is smaller than the corresponding values for $Al_{20}O_{30}$ ANC (5.08 eV) and $Al_{50}O_{75}$ ANT (5.12 eV). Since compounds with larger binding energies have higher stability, the SANC is less stable than the perfect cage and tubular alumina nanomaterials.

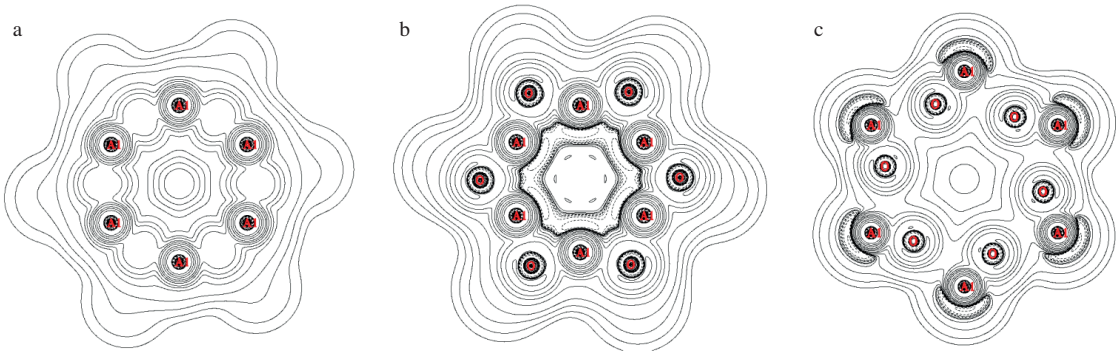

Figure 6. The contour map of electron density Laplacian for the symmetry planes passing through the main adsorption sites of the star-shaped alumina nanocage (sites of Al(I) in the openings of cage (a), sites of Al(II) in the internal pore (b), and sites of Al(III) in the external arms (c)) calculated by CAM-B3LYP/6-31G** level of theory.

The calculated contour map of electron density Laplacian for the symmetry planes passing through the main adsorption sites Al(I–III) of the SANC is shown in Figures 6a–6c. These images describe the difference in distribution of electron density at the openings, internal pore, and external arms of the cage. The natural charge on Al(I) atoms in the openings of the cage is 2.113 $\bar{e}$, which is more positive than the Al(II) atoms in the internal pore (1.330 $\bar{e}$) and the Al(III) atoms in the external arms (0.850 $\bar{e}$). It is possible for these sites to have different activity. To evaluate this characteristic, the interaction of one H_2O molecule with each active site was considered at CAM-B3LYP/6-31G**/LanL2DZ level of theory (Figure 7).

The H_2O molecule has a greater trend to interact with two bridge Al(I) positions of openings from the inside of the cage at a distance of 2.3 Å with the interaction energy (ΔE_{Int}) of –23.8 kcal/mol, or adsorb the top of the Al(I) site of openings at a distance of 2.0 Å with the interaction energy of –36.8 kcal/mol. Energy decomposition analysis of ΔE_{Int} indicates that the contribution of induction energy for these structures is –21.4 and –24.3 kcal/mol, respectively. The sum of exchange repulsion and electrostatic interaction terms is also negative (–2.4 and –12.5 kcal/mol, respectively), suggesting that the exchange repulsion forces are totally quenched by the attractive electrostatic interactions. Meanwhile, adsorption of water over two bridge Al(III) sites on the external arms of SANC at a distance of 2.5 Å is favored by –8.7 kcal/mol energy releasing. The sum of exchange repulsion and electrostatic interaction terms is positive (3.3 kcal/mol). Therefore, the induction term

has the main contribution to the interaction energy of this compound (–12.0 kcal/mol). Molecular adsorption of water over two bridge Al(II) atoms in the internal pore of the SANC at equilibrium distance of 1.9 Å is energetically unfavorable (positive interaction energy). Energy decomposition analysis of ΔE_{Int} (+39.5 kcal/mol) indicates that the negative parts of interaction energy (induction and electrostatic terms) are totally quenched by exchange repulsion, i.e. –144.7 vs. 184.2 kcal/mol. The more negative interaction energy value indicates stronger adsorption of water over the surface. Therefore, the following order is predicted for relative water adsorption activity of aluminum sites of the SANC: Al(I) > Al(III) >>> Al(II).

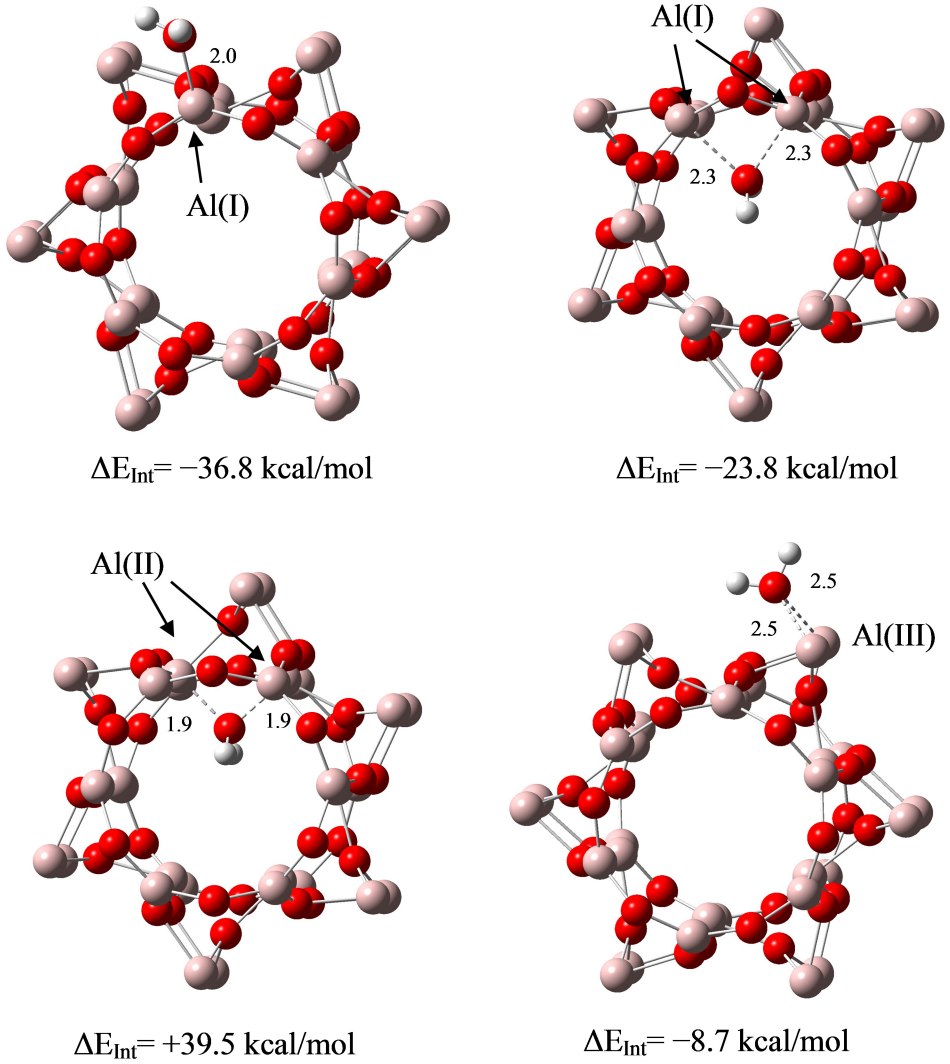

Figure 7. The optimized geometry of the star-shaped alumina nanocage after water adsorption over various aluminum sites calculated by CAM-B3LYP/6-31G**/LanL2DZ level of theory.

H_2O molecule adsorption over the openings of the $Al_{30}O_{30}$ SANC is more favorable than water adsorption over the $Al_{20}O_{30}$ nanocage (–29.3 kcal/mol at equilibrium distance of 2.0 Å) and $Al_{50}O_{75}$ nanotube (–24 to –27 kcal/mol at equilibrium distance of 2.0 Å).[49] These sites also have more negative interaction energy than those reported for molecular adsorption of H_2O over the γ-alumina (100) surface, both experimentally (–19.8

kcal/mol)[55] and theoretically (–19.9 kcal/mol).[46] Therefore, the SANC can be introduced as a novel alumina nanostructure with higher water adsorption activity than well-known alumina compounds.

In summary, the structural and electronic properties as well as water adsorption activity of a novel $Al_{30}O_{30}$ SANC were studied using DFT. These properties were compared to those for the other types of alumina nanomaterials, i.e. $Al_{20}O_{30}$ nanocage and $Al_{50}O_{75}$ nanotube. The electron density of the HOMO and LUMO of the title compound is delocalized inside the cage. These orbitals arise mostly from Al *3s* and *2p* atomic orbitals. The relative strength of the SANC adsorption sites is predicted as openings > external arms >>> internal pore. This compound can be introduced as a novel alumina nanostructure with lower stability and higher activity than other alumina materials.

3. Computation

The Coulomb-attenuating B3LYP method (CAM-B3LYP)[56] was employed for geometry optimization and frequency analysis of the SANC. It was also used to investigate the interaction of H_2O molecule over all active sites of this compound. CAM-B3LYP has a similar quality of B3LYP[57] and performs well for the charge transfer interactions.[56] The Los Alamos relativistic effective core potential plus DZ basis set (LanL2DZ)[58,59] was used for aluminum atoms. The 6-31G** basis set[60] was also applied to oxygen and hydrogen atoms.

The relative stability of various types of alumina nanostructures was determined based on the calculated binding energy per atom in the cluster using Eq. (1), where $E(\mathrm{Al})$, $E(\mathrm{O})$, and $E(\mathrm{Al}_n\mathrm{O}_m)$ are the total energies of Al atom, O atom, and Al_nO_m cluster, and n and m are the number of Al and O atoms in the cluster, respectively.

$$BE/atom = [nE(Al) + mE(O) - E(Al_nO_m)]/(n+m) \tag{1}$$

The basis set superposition error (BSSE) corrected interaction energy (ΔE_{Int}) between the SANC and H_2O was calculated using the Boys–Bernardi counterpoise method[61] through Eq. (2), where E_{SANC} and E_{Water} are the energy of components at the geometry of complex with the basis set of complex. The ΔE_{Int} values were also decomposed into the induction term (ΔE_{Ind}) and the sum of electrostatic and exchange repulsion terms ($\Delta E_{Elst} + \Delta E_{Exch}$), as presented in Eq. (3).

$$\Delta E_{Int} = E_{Complex} - E_{SANC} - E_{Water} \tag{2}$$

$$\Delta E_{Int} = \Delta E_{Ind} + \Delta E_{Elst} + \Delta E_{Exch} \tag{3}$$

Wavefunction analysis[62] was used to study the electronic properties of the SANC, which include the population analysis of molecular orbitals, visualization of electronic contour plots for the HOMO and the LUMO, calculation of the HOMO–LUMO energy gap (ΔE_{gap}), molecular orbital compositions, and DOS. All calculations were performed using the Gaussian-09 software package.[63] The natural population analysis, which includes the calculation of natural atomic charges and natural atomic orbitals (NAO), was carried out using the NBO 3.1 program.[64]

Acknowledgments

The author is grateful to the research council of Damghan University. This article is dedicated to Prof Houshang Jamshid Foroudian, emeritus professor of organic chemistry from Isfahan University, on the occasion of his 75th birthday.

References

1. Tenne, R. *Chem. Eur. J.* **2002**, *8*, 5296–5304.
2. Tenne, R. *Angew. Chem. Int. Ed.* **2003**, *42*, 5124–5132.
3. Tenne, R.; Redlich, M. *Chem. Soc. Rev.* **2010**, *39*, 1423–1434.
4. Adini, A. R.; Redlich, M.; Tenne, R. *J. Mater. Chem.* **2011**, *21*, 15121–15131.
5. Bar-Sadan, M.; Tenne, R. In *Inorganic Nanoparticles: Synthesis, Applications, and Perspectives*; Altavilla, C.; Ciliberto, E., Eds. CRC Press, Taylor & Francis Group: Boca Raton, FL, USA, 2011, pp. 441–474.
6. Catlow, C. R. A.; Bromley, S. T.; Hamad, S.; Mora-Fonz, M.; Sokol, A. A.; Woodley, S. M. *Phys. Chem. Chem. Phys.* **2010**, *12*, 786–811.
7. Bromley, S. T.; Moreira, I. D. P. R.; Neyman, K. M.; Illas, F. *Chem. Soc. Rev.* **2009**, *38*, 2657–2670.
8. Tenne, R. In *Nanotubes and Nanofibers*; Gogotsi, Y., Ed. CRC Press, Taylor & Francis Group: Boca Raton, FL, USA, 2006, pp. 135–177.
9. Tenne, R.; Remskar, M.; Enyashin, A.; Seifert, G. *Top. Appl. Phys.* **2008**, *111*, 631–671.
10. Rao, C. N. R.; Nath, M. *Dalton Trans.* **2003**, 1–24.
11. Rao, C. N. R.; Govindaraj, A.; Vivekchand, S. R. C. *Annu. Rep. Prog. Chem. Sect. A* **2006**, *102*, 20–45.
12. Rao, C. N. R.; Govindaraj, A. In *Advanced Nanomaterials*; Geckeler, K. E.; Nishide, H., Eds. Wiley-VCH Verlag: Weinheim, Germany, 2010, pp. 195–247.
13. Golberg, D.; Terrones, M. In *Carbon Meta-Nanotubes: Synthesis, Properties and Applications*; Monthioux, M., Ed. John Wiley & Sons: Chichester, UK, 2012, pp. 323–409.
14. Chang, C.; Patzer, B.; Sulzle, D. In *Handbook of Nanophysics: Clusters and Fullerenes*; Sattler, K. D., Ed. CRC Press, Taylor & Francis Group: Boca Raton, FL, USA, 2011, pp. 51–113.
15. Kim, Y.; Kim, C.; Kim, P.; Yi, J. *J. Non-Cryst. Solid.* **2005**, *351*, 550–556.
16. Rozita, Y.; Brydson, R.; Scott, A. J. *J. Phys. Conference Series* **2010**, *241*, 012096.
17. Geng, D. Y.; Zhang, Z. D.; Zhang, W. S.; Si, P. Z.; Zhao, X. G.; Liu, W.; Hu, K. Y.; Jin, Z. X. *Scripta Mater.* **2003**, *48*, 593–598.
18. Zhou, J.; He, J.; Zhao, G.; Zhang, C.; Zhao, J.; Hu, H. *Trans. Nonferrous. Met. Soc. China* **2007**, *17*, 82–86.
19. Zhou, J.; Deng, S. Z.; Chen, J.; She, J. C.; Xu, N. S. *Chem. Phys. Lett.* **2002**, *365*, 505–508.
20. Ma, M.; Zhu, Y.; Xu, Z. *Mater. Lett.* **2006**, *61*, 1812–1815.
21. Dabbagh, H. A.; Rasti, E.; Yalfani, M. S.; Medina, F. *Mater. Res. Bull.* **2011**, *46*, 271–277.
22. Masuda, H.; Yamada, H.; Satoh, M.; Asoh, H.; Nakao, M.; Tamamura, T. *Appl. Phys. Lett.* **1997**, *71*, 2770–2772.
23. Pu, L.; Bao, X. M.; Zou, J. P.; Feng, D. *Angew. Chem. Int. Ed.* **2001**, *40*, 1490–1493.
24. Zou, J.; Pu, L.; Bao, X.; Feng, D. *Appl. Phys. Lett.* **2002**, *80*, 1079–1081.
25. Mei, Y. F.; Wu, X. L.; Shao, X. F.; Siu, G. G.; Bao, X. M. *Europhys. Lett.* **2003**, *62*, 595–599.
26. Mei, Y. F.; Wu, X. L.; Shao, X. F.; Huang, G. S.; Siu, G. G. *Phys. Lett. A* **2003**, *309*, 109–113.
27. Lee, W.; Scholz, R.; Gosele, U. *Nano Lett.* **2008**, *8*, 2155–2160.
28. Xiao, Z. L.; Han, C. Y.; Welp, U.; Wang, H. H.; Kwok, W. K.; Willing, G. A.; Hiller, J. M.; Cook, R. E.; Miller, D. J.; Crabtree, G. W. *Nano Lett.* **2002**, *2*, 1293–1297.
29. Hwang, J.; Min, B.; Lee, J. S.; Keem, K.; Cho, K.; Sung, M. Y.; Lee, M. S.; Kim, S. *Adv. Mater.* **2004**, *16*, 422–425.
30. Lee, J. S.; Min, B.; Cho, K.; Kim, S.; Park, J.; Lee, Y. T.; Kim, N. S.; Lee, M. S.; Park, S. O.; Moon, J. T. *J. Cryst. Growth* **2003**, *254*, 443–448.
31. Wakihara, T.; Hirasaki, T.; Shinoda, M.; Meguro, T.; Tatami, J.; Komeya, K.; Inagaki, S.; Kubota, Y. *Cryst. Growth Des.* **2009**, *9*, 1260–1263.

32. Zhang, Y.; Liu, J.; He, R.; Zhang, Q.; Zhang, X.; Zhu, J. *Chem. Phys. Lett.* **2002**, *360*, 579–584.
33. Ogihara, H.; Sadakane, M.; Nodasaka, Y.; Ueda, W. *Chem. Mater.* **2006**, *18*, 4981–4983.
34. Fontes Diniz, C.; Balzuweit, K.; Della Santina Mohallem, N. *J. Nanoparticle Res.* **2007**, *9*, 293–300.
35. Qu, L.; He, C.; Yang, Y.; He, Y.; Liu, Z. *Mater. Lett.* **2005**, *59*, 4034–4037.
36. Lu, C. L.; Lv, J. G.; Xu, L.; Guo, X. F.; Hou, W. H.; Hu, Y.; Huang, H. *Nanotechnology* **2009**, *20*, 215604.
37. Rahane, A. B.; Deshpande, M. D.; Kumar, V. *J. Phys. Chem. C* **2011**, *115*, 18111–18121.
38. Li, R.; Cheng, L. *Comput. Theoret. Chem.* **2012**, *996*, 125–131.
39. Woodley, S. M. *Proc. R. Soc. A* **2011**, *467*, 2020–2042.
40. Sun, J.; Lu, W. C.; Zhang, W.; Zhao, L. Z.; Li, Z. S.; Sun, C. C. *Inorg. Chem.* **2008**, *47*, 2274–2279.
41. Gu, Y. B.; Di, Q.; Lin, M. H.; Tan, K. *Comput. Theoret. Chem.* **2012**, *981*, 86–89.
42. Linnolahti, M.; Pakkanen, T. A. *Inorg. Chem.* **2004**, *43*, 1184–1189.
43. Charkin, O. P.; Klimenko, N. M.; Charkin, D. O. *Russ. J. Inorg. Chem.* **2008**, *53*, 568–578.
44. Zheng, X.; Zhang, Y.; Huang, S.; Liu, H.; Wang, P.; Tian, H. *Appl. Surf. Sci.* **2011**, *257*, 6410–6417.
45. Dabbagh, H. A.; Taban, K.; Zamani, M. *J. Mol. Catal. A: Chem.* **2010**, *326*, 55–68.
46. Dabbagh, H. A.; Zamani, M.; Davis, B. H. *J. Mol. Catal. A: Chem.* **2010**, *333*, 54–68.
47. Zamani, M.; Dabbagh, H. A. *J. Nanoanal.* **2014**, *1*, 21–30.
48. Dabbagh, H. A.; Zamani, M.; Farrokhpour, H.; Namazian, M.; Etedali Habibabadi, H. *Chem. Phys. Lett.* **2010**, *485*, 176–182.
49. Dabbagh, H. A.; Zamani, M. *Comput. Mater. Sci.* **2013**, *79*, 781–788.
50. Oziminski, W. P.; Garnuszek, P.; Bednarek, E.; Dobrowolski, J. Cz. *Inorg. Chim. Acta.* **2007**, *360*, 1902–1914.
51. Ealet, B.; Elyakhloufi, M. H.; Gillet, E.; Ricci, M. *Thin Solid Films* **1994**, *250*, 92–100.
52. French, H. *J. Am. Ceram. Soc.* **1990**, *73*, 477–489.
53. Flores-Hidalgo, M. A.; Barraza-Jiménez, D.; Glossman-Mitnik, D. *Comput. Theoret. Chem.* **2011**, *965*, 154–162.
54. Sriram, S.; Chandiramouli, R.; Thayumanavan, A. *Adv. Mat. Lett.* **2015**, *6*, 446–451.
55. Gatta, G. D.; Fubini, B.; Stradella, L. *J. Chem. Soc. Faraday. Trans.* **1977**, *73*, 1040–1049.
56. Yanai, T.; Tew, D. P.; Handy, N. C. *Chem. Phys. Lett.* **2004**, *393*, 51–57.
57. Becke, A. D. *J. Chem. Phys.* **1993**, *98*, 5648-5652.
58. Wadt, W. R.; Hay, P. J. *J. Chem. Phys.* **1985**, *82*, 284–298.
59. Hay, P. J.; Wadt, W. R. *J. Chem. Phys.* **1985**, *82*, 299–310.
60. Krishnan, R.; Binkley, J. S.; Seeger, R.; Pople, J. A. *J. Chem. Phys.* **1980**, *72*, 650–654.
61. Boys, S. F.; Bernardi, F. *Mol. Phys.* **1970**, *19*, 553–566.
62. Lu, T.; Chen, F. *J. Comp. Chem.* **2012**, *33*, 580–592.
63. Frisch, M. J.; Trucks, G. W.; Schlegel, H. B.; Scuseria, G. E.; Robb, M. A.; Cheeseman, J. R.; Montgomery Jr., J. A.; Vreven, T.; Kudin, K. N.; Burant, J. C.; et al. *Gaussian 09*, *Revision A02*, Gaussian, Inc.: Wallingford, CT, USA, 2009.
64. Glendening, E. D.; Carpenter, A. E.; Reed, A. E.; Weinhold, F. *NBO*, *Version 3.1*, University of Wisconsin: WI, USA, 1995.